JOURNAL OF COMPUTATIONAL PHYSICS **126,** 421–433 (1996)
ARTICLE NO. 0147

A Conservative Shock Fitting Method on Unstructured Grids

J.-Y. TRÉPANIER, M. PARASCHIVOIU, M. REGGIO, AND R. CAMARERO

Département de génie mécanique, École Polytechnique de Montréal, C.P. 6079, succursale Centre-ville, Montréal, Québec, Canada H3C 3A7

Received February 6, 1995; revised December 13, 1995

A dynamic discontinuity tracking method to achieve shock fitting is presented. The method is based on the properties of Roe's scheme which becomes an exact Riemann solver when grid lines are aligned with the discontinuity. To make full use of this property, a technique that moves and adapts the grid in order to align and position element interfaces on the discontinuities is proposed. This algorithm is implemented with a conventional two-dimensional finite volume solver on unstructured triangular meshes. The method's ability to retrieve the exact solution is investigated on simple problems having analytical solutions.

1. INTRODUCTION

The treatment of discontinuities such as shock waves has been a persistent problem in the numerical simulation of compressible flows. The initial approaches consisted in treating shocks explicitly and were relatively straightforward when the discontinuity could be taken as a boundary of the computational domain [1]. For example, in the supersonic flow over a blunt body, a normalisation of the domain between the body and the shock through a coordinate transformation produces a curvilinear grid where the shock fits one of the boundaries. With a known uniform upstream flow and the Rankine–Hugoniot relations, the shock can then be computed exactly. More complex flows with embedded shocks and interactions producing reflections, as well as contact surfaces and gradient discontinuities, requires managing complicated topology in an ad-hoc fashion. In attempting to devise generic solution procedures, two approaches have evolved: the shock-fitting and the shock-capturing techniques. The early controversy [1] centered about two issues:

- the goal of a single integration scheme capable of predicting and computing discontinuities without special treatment versus the logical difficulties and associated programming hurdles of fitting shocks;
- the requirements of accuracy and correct behaviour in the vicinity of discontinuities versus efficiency both from memory and computation requirements.

The shock capturing approach based on the conservative form of the Euler equations, together with appropriate upwinding schemes, has met with great success the first objective and only partially the second. The weakness of this approach being that the shocks are captured over several grid points. While the sharpness of these discontinuities can be improved by refining the grid in the vicinity of these regions, this leads to high computing costs due to the large number of elements and the decrease of the global time step particularly in three space dimensions. The shock-fitting approach and recent variants such as the λ-scheme have fared better in achieving good accuracy while encountering severe limitations on the topology of interaction patterns. A recent assessment of the situation is given in Ref. [2].

Resolving these problems requires addressing some fundamental and technological issues relating to the correct computation of shock discontinuities and their detection. Until recently it was felt that applying the Rankine–Hugoniot relations was the only way to achieve the exact jump conditions. With the Roe scheme, it is possible, although this is not generally appreciated, to obtain the exact jump, provided the shock and the cell face are aligned [3–5]. The problem of detection of the onset of a shock and its tracking does not have rigourous foundations and is still largely based on heuristics [4]. An appropriate model for the wave propagation phenomena has been proposed in [6]. In this model three basic waves are identified and relations to compute their directions and strengths from the basic flow variables are given. From this, it is possible to extract information from the computed flow field and to use it to align the mesh locally. Coupled with a grid adaptation algorithm, this model can drive a local grid alignment procedure allowing the correct jump calculation and sharp shock resolution by the Roe scheme.

In the present paper, a methodology to perform these tasks is proposed. It is based on a formulation of the Euler equations in a Lagrangian–Eulerian reference frame, and an approximate Riemann solver appropriately modified for the motion of the mesh. The detection techniques of the flow features used to adapt the mesh are derived from a wave model. These provide the link to the adaptive algorithms to align and move the grid edges along discontinuities. Finally, the methodology has been validated and results for analytical test cases are presented.

0021-9991/96 $18.00

2. THE SOLVER

2.1. *The Equations*

The mathematical model for inviscid and adiabatic flows is the Euler system of equations representing the conservation of mass, of momentum, and of energy. The integral form of these equations for an arbitrary Lagrangian–Eulerian referential frame can be written as

$$\frac{\partial}{\partial t}\int_{V(t)} U dV + \oint_{S(t)} \mathbf{n}\cdot\mathbf{F}\, dS = 0, \tag{1}$$

where $\mathbf{n}$ is the outward unit vector normal to the boundary $S(t)$, which encloses the time-dependent volume $V(t)$. The vector of dependent variables U and the flux tensor $\mathbf{F}$ are

$$U = \begin{bmatrix} \rho \\ \rho\mathbf{u} \\ \rho E \end{bmatrix}, \quad \mathbf{F} = \begin{bmatrix} \rho(\mathbf{u}-\mathbf{w}) \\ \rho(\mathbf{u}-\mathbf{w})\mathbf{u} + \mathbf{I}p \\ \rho(\mathbf{u}-\mathbf{w})E + \mathbf{u}p \end{bmatrix}, \tag{2}$$

where ρ represents the density, $\mathbf{u}$ the fluid velocity, $\mathbf{w}$ the velocity of the boundary of the volume, E the specific total energy, p the pressure, and $\mathbf{I}$ the metric tensor. This system is completed by the equation of state for a perfect gas,

$$p = (\gamma-1)\rho\left(E - \frac{1}{2}\mathbf{u}\cdot\mathbf{u}\right), \tag{3}$$

where γ is a constant representing the ratio of specific heat capacities of the fluid.

2.2. *The Scheme*

A finite-volume scheme to solve these equations has been described in [7]. Applying this approach on an unstructured triangular discretisation gives the following expression to advance the solution $\mathbf{U}$ in time:

$$U^{n+1}V^{n+1} - U^nV^n = -\sum_{k=1}^{N\,\text{gides}} \mathbf{F}. \tag{4}$$

The flux, F, between adjacent cells can be expressed as

$$F = \frac{1}{2}\left[F_\mathrm{r} + F_\mathrm{l} - \sum_{i=1}^{4} \alpha_i |\Lambda_i| e_i \right], \tag{5}$$

where the subscripts r and l denote the right and left states at the interface. In this expression the flux difference across a cell face represents the contribution of four waves: two acoustics, one entropy, and one shear. All the waves are assumed to move in the normal direction to the edge. The left and right fluxes on each side of the interface during a time interval Δt are defined as

$$F = \begin{bmatrix} \rho u_n^* \\ \rho u u_n^* - p\sin\theta \\ \rho v u_n^* + p\cos\theta \\ \rho E u_n^* + p u_n \end{bmatrix}_{l,r} S\,\Delta t \tag{6}$$

with $u_n^* = u_n - w_{nr}$ and $u_n = -u\sin\theta + v\cos\theta$.

In these expressions, θ denotes the angle between the x coordinate and the normal to the face. The flux eigenvalues are given by

$$\Lambda = \begin{bmatrix} u_n^* + a \\ u_n^* - a \\ u_n^* \\ u_n^* \end{bmatrix} S\,\Delta t, \tag{7}$$

where S represents the length of the edge and a is the speed of sound. The flow variables u, v, a, and p are evaluated using Roe's average which introduces the average jacobian $\overline{A}$ to approximate the jacobian $A = \partial F/\partial U$. The average state for the matrix $\overline{A}$ has been proposed by Roe [5] to satisfy the following properties:

1. $\overline{A}$ constitutes a linear mapping form the vector space U to the vector space $\mathbf{F}$.
2. As $U_\mathrm{l} \to U_\mathrm{r} \to U$, $\overline{A}(U_\mathrm{l}, U_\mathrm{r}) \to A(U)$.
3. $\overline{A}(U_\mathrm{l}, U_\mathrm{r})\,(U_\mathrm{l} - U_\mathrm{r}) = \mathbf{F_l} - \mathbf{F_r}$.
4. The eigenvalues of $\overline{A}$ are linearly independent.

Property 3 is the most important in the present context since it implies a discrete imposition of the Rankine–Hugoniot relations for steady or moving discontinuities.

Based on these constraints, Roe's average variables are defined by

$$\begin{aligned} \overline{\rho} &= \sqrt{\rho_\mathrm{l}\rho_\mathrm{r}} \\ \overline{\phi} &= \frac{\sqrt{\rho_\mathrm{r}}\phi_\mathrm{r} + \sqrt{\rho_\mathrm{l}}\phi_\mathrm{l}}{\sqrt{\rho_\mathrm{r}} + \sqrt{\rho_\mathrm{l}}}, \quad \overline{\phi} = \overline{u}, \overline{v}, \overline{h}. \end{aligned} \tag{8}$$

This average state linearizes the Riemann problem at each interface. The expressions for the eigenvectors components $\mathbf{e_i}$ are documented in Ref. [5]. The solution to the approximate Riemann problem can be given as a summation of the average right eigenvector $\mathbf{e_i}$ and wave

strength α_i:

$$U_l - U_r = \sum_{i=1}^{4} \alpha_i \mathbf{e_i}. \tag{9}$$

By solving this equation, the wave strengths α_i are obtained:

$$\alpha_i = \begin{bmatrix} \frac{1}{2a^2}(\Delta p + \rho a \Delta u_n) \\ \frac{1}{2a^2}(\Delta p - \rho a \Delta u_n) \\ \Delta\rho - \frac{1}{a^2}\Delta p \\ \rho \Delta u_t \end{bmatrix}. \tag{10}$$

As described in Ref. [8] and in order to satisfy the geometric conservation laws, the normal velocity of the face w_n must be specified geometrically by a relation involving a volume increment ΔV along each one of its sides. This is such that

$$w_n = \frac{\Delta V}{S\,\Delta t}. \tag{11}$$

3. DETECTION OF FLOW FEATURES

3.1. *The Wave Model*

The basic idea in the present dynamic discontinuity tracking (DDT) method is to adapt dynamically the mesh to fit discontinuities in the flow. This involves two fundamental capabilities: the first is to detect accurately the various wave patterns of the flow; the second is to perform the required actions on the grid to align it with discontinuities. The adjustment of the grid must be carried out without perturbing the solution because the method is to be applied to unsteady flows and because the convergence of the process will be improved if unphysical perturbations are avoided.

Feature detection is performed using the wave model proposed by Roe [6], where it is assumed that the flow variables are locally represented as a linear superposition of elementary solutions of the Euler equations written in primitive variables:

$$\mathbf{W} = [p, u, v, \rho]^{\mathrm{T}} \tag{12}$$

Such a superposition can be written as

$$\mathbf{W} = \sum \alpha_i(\theta)\mathbf{e_i}(\theta)\,(x\cos(\theta) + y\sin(\theta) - \lambda_i(\theta)t), \tag{13}$$

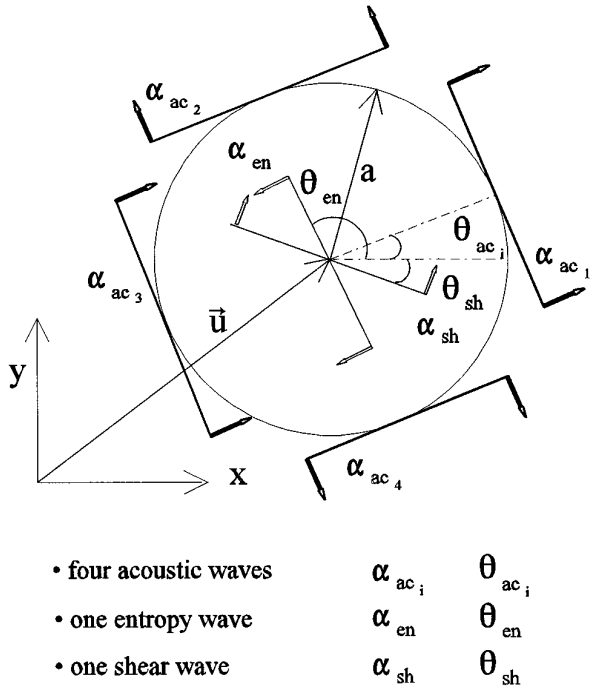

FIG. 1. Model for wave detection.

where θ is the wave angle which changes from wave to wave.

The design of physically meaningful wave models depends on the choice of a number of parameters and their combination. Essentially, from Eq. (13), the eigenvectors are first selected such as to represent the basic phenomena observed in inviscid compressible flows. Three types of waves are needed: acoustic waves, shear waves, and entropy waves. The corresponding three eigenvectors are given in Ref. [6]. Furthermore, there remains some freedom on how to choose the number of each type of wave and their relative orientation. This depends on the goal of the model. For the purpose of the identification of flow features, it was found adequate to combine a set of four orthogonal acoustic waves, one shear wave, and one entropy as shown in Fig. 1. The four acoustic waves propagate along orthogonal directions with $|\theta_{\mathrm{ac}_1}| < \pi/4$ taken as the reference. The shear and entropy waves propagate respectively in the directions θ_{sh} and θ_{en}.

Considering the contribution of these waves, the derivatives of the primitive variables may be written as

$$\rho_x = \sum_{i=1}^{4} \rho\,\alpha_{\mathrm{ac}_i}\cos\theta_{\mathrm{ac}_i} + \rho\,\alpha_{\mathrm{en}}\cos\theta_{\mathrm{en}} \tag{14a}$$

$$\rho_y = \sum_{i=1}^{4} \rho\,\alpha_{\mathrm{ac}_i}\sin\theta_{\mathrm{ac}_i} + \rho\,\alpha_{\mathrm{en}}\sin\theta_{\mathrm{en}} \tag{14b}$$

$$u_x = \sum_{i=1}^{4} a\alpha_{\mathrm{ac}_i}\cos^2\theta_{\mathrm{ac}_i} - \alpha_{\mathrm{sh}} a \sin\theta_{\mathrm{sh}}\cos\theta_{\mathrm{sh}} \tag{14c}$$

$$u_y = \sum_{i=1}^{4} a\alpha_{\mathrm{ac}_i}\cos\theta_{\mathrm{ac}_i}\sin\theta_{\mathrm{ac}_i} - \alpha_{\mathrm{sh}} a \sin^2\theta_{\mathrm{sh}} \tag{14d}$$

$$v_x = \sum_{i=1}^{4} \alpha_{\mathrm{ac}_i} a \sin\theta_{\mathrm{ac}_i}\cos\theta_{\mathrm{ac}_i} + \alpha_{\mathrm{sh}} a \cos^2\theta_{\mathrm{sh}} \tag{14e}$$

$$v_y = \sum_{i=1}^{4} \alpha_{\mathrm{ac}_i} a \sin^2\theta_{\mathrm{ac}_i} + \alpha_{\mathrm{sh}} a \sin\theta_{\mathrm{sh}}\cos\theta_{\mathrm{sh}} \tag{14f}$$

$$p_x = \sum_{i=1}^{4} \rho a^2 \alpha_{\mathrm{ac}_i}\cos\theta_{\mathrm{ac}_i} \tag{14g}$$

$$p_y = \sum_{i=1}^{4} \rho a^2 \alpha_{\mathrm{ac}_i}\cos\theta_{\mathrm{ac}_i}. \tag{14h}$$

Solving this system of equations gives the following wave angles and strengths:

$$\theta_{\mathrm{en}} = \tan^{-1}\frac{a^2\rho_y - p_y}{a^2\rho_x - p_x}$$

$$\theta_{\mathrm{sh}} = \theta_{\mathrm{ac}_1} - \frac{\pi}{4}\,\mathrm{sgn}(v_x - u_y)$$

$$\theta_{\mathrm{ac}_1} = \frac{1}{2}\tan^{-1}\frac{v_x + u_y}{u_x - v_y}$$

$$\theta_{\mathrm{ac}_2} = \theta_{\mathrm{ac}_1} + \pi$$

$$\theta_{\mathrm{ac}_3} = \theta_{\mathrm{ac}_1} + \frac{\pi}{2}$$

$$\theta_{\mathrm{ac}_4} = \theta_{\mathrm{ac}_1} - \frac{\pi}{2}; \tag{15}$$

$$\alpha_{\mathrm{an}} = \frac{1}{\rho a^2}\sqrt{(a^2\rho_x - p_x)^2 + (a^2\rho_y - p_y)^2} \tag{16a}$$

$$\alpha_{\mathrm{sh}} = \frac{v_x - u_y}{a} \tag{16b}$$

$$\alpha_{\mathrm{ac}_1} = \frac{1}{2}\left[\frac{u_x + v_y + R + a\alpha_{\mathrm{sh}}}{2a} + \frac{p_x\cos\theta_{\mathrm{ac}_1} + p_y\sin\theta_{\mathrm{ac}_1}}{\rho a^2}\right] \tag{16c}$$

$$\alpha_{\mathrm{ac}_2} = \frac{1}{2}\left[\frac{u_x + v_y + R + a\alpha_{\mathrm{sh}}}{2a} - \frac{p_x\cos\theta_{\mathrm{ac}_1} + p_y\sin\theta_{\mathrm{ac}_1}}{\rho a^2}\right] \tag{16d}$$

$$\alpha_{\mathrm{ac}_3} = \frac{1}{2}\left[\frac{u_x + v_y - R - a\alpha_{\mathrm{sh}}}{2a} - \frac{p_x\sin\theta_{\mathrm{ac}_1} - p_y\cos\theta_{\mathrm{ac}_1}}{\rho a^2}\right]; \tag{16e}$$

$$R = \mathrm{sgn}(u_x - v_y)\sqrt{(v_x + u_y)^2 + (u_x - v_y)^2}. \tag{17}$$

This model has demonstrated its accuracy in the capture of oblique shock waves as well as contact discontinuities. A full description of this wave model is found in Ref. [6].

The computation of the wave strengths and angles requires the flow gradients. These values are computed at the triangle center using a standard Gauss quadrature involving the values of the variables at elements sharing a common node with the considered triangle.

3.2. *Identification of the Flow Features*

The wave model used in this study is based on a superposition of linear waves and is not capable of representing genuinely non-linear waves and discontinuities. But this is not critical because it is not used for that purpose. What is required is the ability to detect a dominant wave and its angle of propagation. When the model is applied in regions of discontinuities such as shocks or slip lines, the flow features will be roughly represented by the model. More specifically, a shock wave will be seen as a strong acoustic wave, a slip line will be represented by a shear wave, and a moving contact discontinuity as an entropy wave. This correspondence is the basis of the detection algorithm.

The detection process involves the filtering of the waves which comprises two operations. First, the weak waves are discarded, according to the relative strength of each wave. The criteria for this step has been fixed at 10% of the maximum wave intensity over the whole domain. Second, only one wave is retained for each triangle. The criteria here is that a wave is retained if its has a strength of an order of magnitude greater than the other waves in the same element.

After this process, most of the triangles will have their waves discarded, except those triangles near discontinuities, dividing the whole triangulation in two groups: the

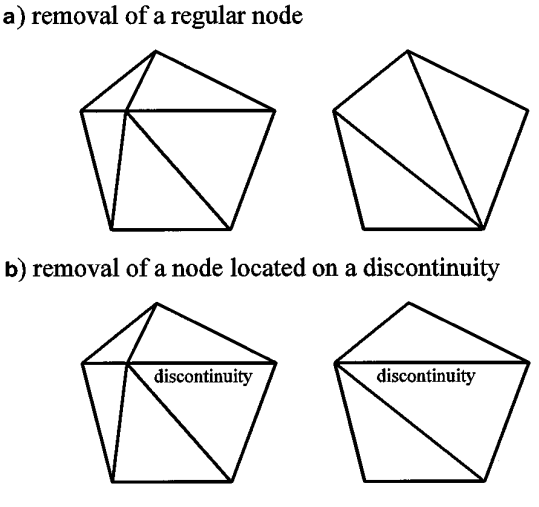

FIG. 2. Coarse-cure procedure: (a) removal of a regular node; (b) removal of a node located on a discontinuity.

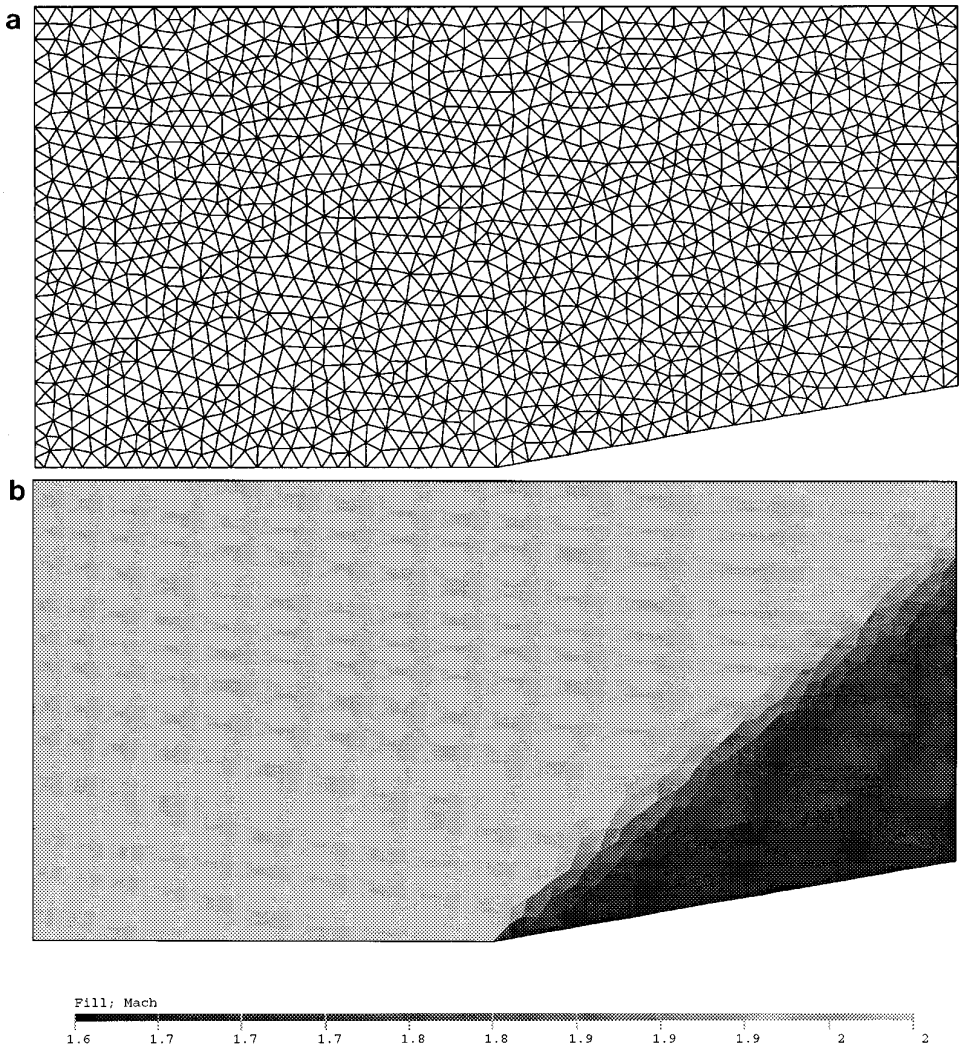

FIG. 3. Initial grid and Mach number distribution for the wedge computation.

active group comprising triangles with only one strong wave and the non-active group comprising triangles without a dominant wave.

4. GRID MANAGEMENT

The grid management is a critical aspect of the DDT algorithm. It is performed with three basic actions: (i) orientation of some edges of the triangulation to align them in a direction perpendicular to the wave direction; (ii) translation of the edges to follow moving discontinuities; and (iii) removal of ill-shaped triangles. In addition, a grid adaptation procedure can be superimposed on these algorithms.

4.1. *Orientation of the Edges*

The procedure for the orientation of the edges is applied to the set of triangles for which a dominant wave has been identified. This set of triangles has been called the active group. Only the orientation of this dominant wave is used to modify the grid. The list of triangles in the active group is converted into a list of active edges as follows. For each triangle, an edge which is the most perpendicular to the dominant wave is selected; and an edge becomes active only if it is selected by its two neighbor triangles. With this list of active edges, an attempt is made to orient these edges perpendicularly to the dominant wave. As conflicting requirements can result from different wave directions, this is carried out globally through an optimisation procedure. The technique is similar to that described in Ref. [10] but a different objective function is used to align the grid. This objective function sums the vector product between the normalized wave orientation vector and the normalized edge vector. Details can be found in Ref. [11]. The minimization of the objective function is performed using a gradient method based on the steepest descent technique.

4.2. *Translation of the Edges*

Once the edges have been aligned normal to the dominant waves, a translation is needed to move the edges directly on the shock or slip lines. The translation velocity is obtained by adding to both nodes of every active edge the velocity of the dominant wave in the direction detected by the wave model. For this action, the velocity of the wave computed with the standard grid-aligned Roe's scheme is used since the edge is now almost perpendicular to the dominant wave, implying that the computed wave velocity satisfies the Rankine–Hugoniot relation. For steady discontinuities the movement converges to an accurate positioning of the edges directly on the discontinuities. For unsteady flows, the velocity obtained at each node is the sum of two velocities, one of which follows the normal movement of the discontinuity and the other that rotates the edge about the discontinuity.

4.3. *Grid Cure and Adaptation*

The alignment and translation of the active edges define a grid velocity **w** which gradually deforms the triangulation and aligns some edges along the main discontinuities. However, during the motion, some triangles can degenerate. Curing these problems dynamically without introducing strong perturbations is critical in the DDT algorithm.

The basic set of actions used to modify the grid have been described in Ref. [9] in the context of a grid generation package. One of these is the coarse-cure step which consists in removing one node of a badly shaped triangle and to remesh the open polygon. This is illustrated on Fig. 2a. Badly shaped triangles are identified by computing a quality parameter for each triangle which measures the equilaterality of the triangle. This quality is defined as

$$Q = \frac{4\sqrt{3}\,\text{Area}}{a^2 + b^2 + c^2},$$

where "Area" is the area of the triangle and a, b, and c are the lengths of its three edges. This quality is equal to 1 for an equilateral triangle and goes to zero for a degenerate one. In the present implementation, a triangle is considered ill-shaped if Q is lower than 0.3.

Special care must be taken when removing a node lying on a discontinuity. In such a case, the remeshing of the polygon must be done so as to retrieve the discontinuity as a mesh line. This is illustrated in Fig. 2b. This is possible only if the remeshing procedure receives some information from the feature detection procedure identifying the lines of discontinuity.

In addition, the grid management can be coupled with an adaptativity methodology. The only restriction in this case is again to prohibit removal of the sides located along discontinuities, so as to preserve the well-positioned interfaces.

4.4. *Global Algorithm*

The DDT algorithm can be summarized as follows: For each time step

- compute the wave strengths and directions from the wave model described in Section 3,
- compute the grid velocity from translation and rotation actions as described in Sections 4.1 and 4.2,
- advance the solution one time step using the moving grid flow solver, as described in Section 2,
- apply the grid cure algorithm to remove badly shaped triangles, as described in Section 4.3,
- modify the grid using adaptation (if needed).

5. RESULTS

5.1. *Flow over a Single Wedge*

This first test case will be used to validate the method. It consists of a Mach 2 flow incident over a 10° wedge. The

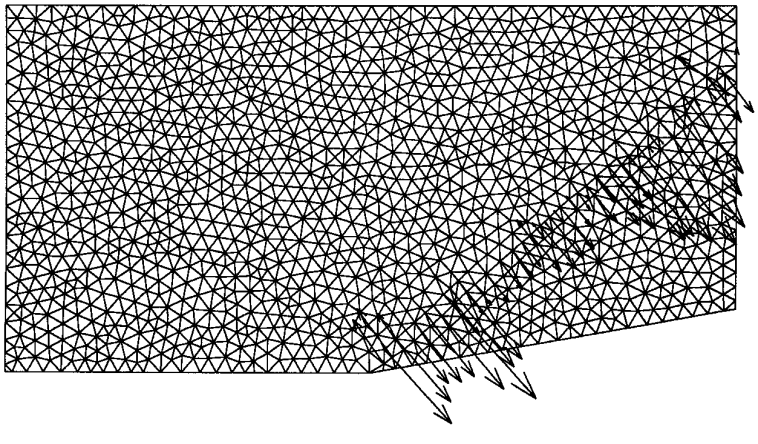

FIG. 4. Grid and grid velocity after a few time steps of the DDT algorithm.

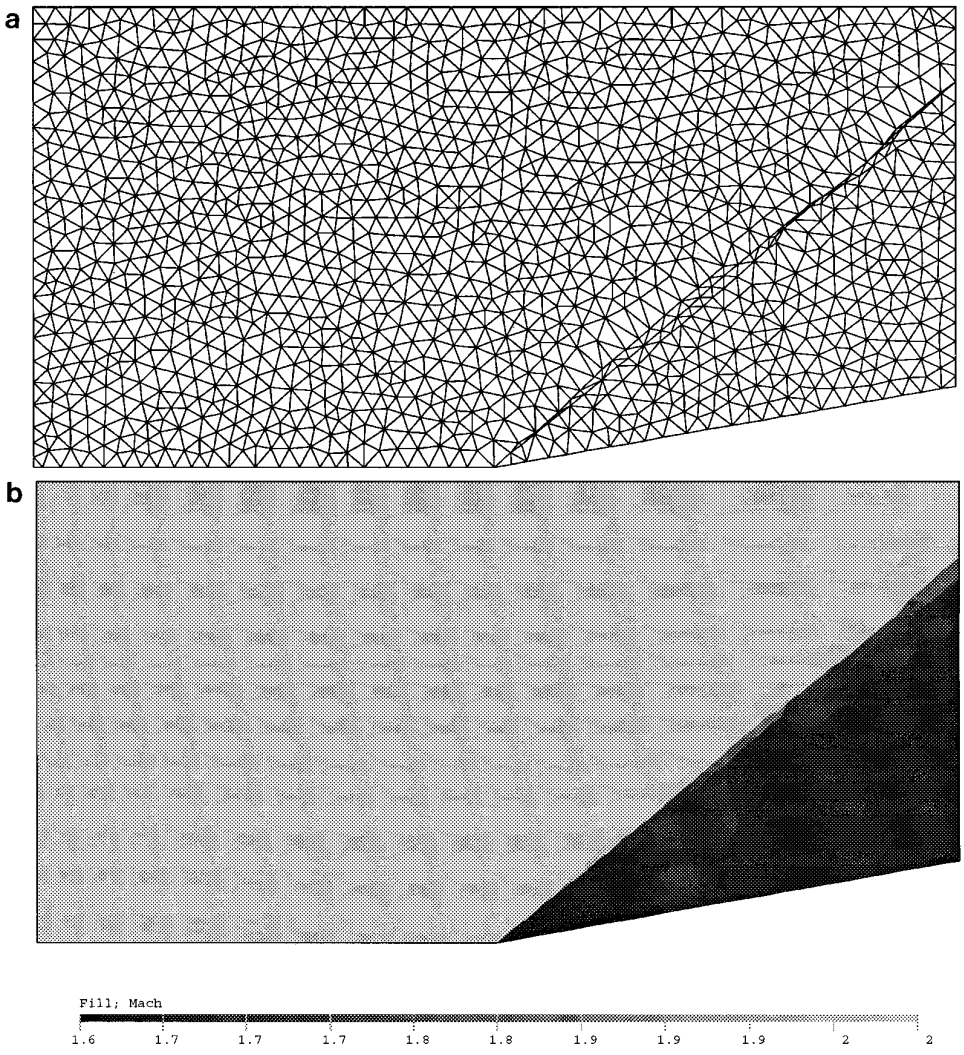

FIG. 5. Converged grid and Mach number distribution using the DDT algorithm and a fixed connectivity.

effect of the various actions involved in the process of grid management has been investigated in a systematic way. The starting point for all cases is the grid and solution represented on Fig. 3. The oblique shock wave captured by the scheme extends over approximately two to three cells. In a first computation, the DDT method was used to compute the grid velocity but the grid connectivity was kept as the grid nodes move. After a few time steps, the grid translation and rotation algorithms have almost succeeded in aligning the grid with the shock wave. This is illustrated on Fig. 4, together with the current grid velocity, as computed by the DDT algorithm.

After a few hundred time steps, some triangles tend to degenerate along the shock line, as shown in Fig. 5a. This is attributable to the translation grid velocities which attempt to bring grid points from both side of the shock towards the shock position. At this point, the algorithm almost stops due to the time step limitation given by the CFL criteria. The Mach number distribution obtained is represented on Fig. 5b. It can be appreciated on this figure that even if the algorithm stops because of a degenerated triangle, the overall solution is improved compared to the initial one.

Further improvements are straightforward if one allows for some cure action of the grid as described in Section 4.3. This is illustrated in a second computation, where the grid is checked every 10 time steps for low quality triangles and these are removed by the coarse-cure action. The actions on the grid are thus limited to node removal and the result is that the number of grid nodes will be reduced as the grid is cured.

The results obtained with this procedure are shown on Figs. 6a and 6b. Figure 6a illustrates the grid obtained after a few hundred iterations. One can see the ability of the method to align the sides of the control volumes with the shock. However, as the grid becomes coarser, the ability

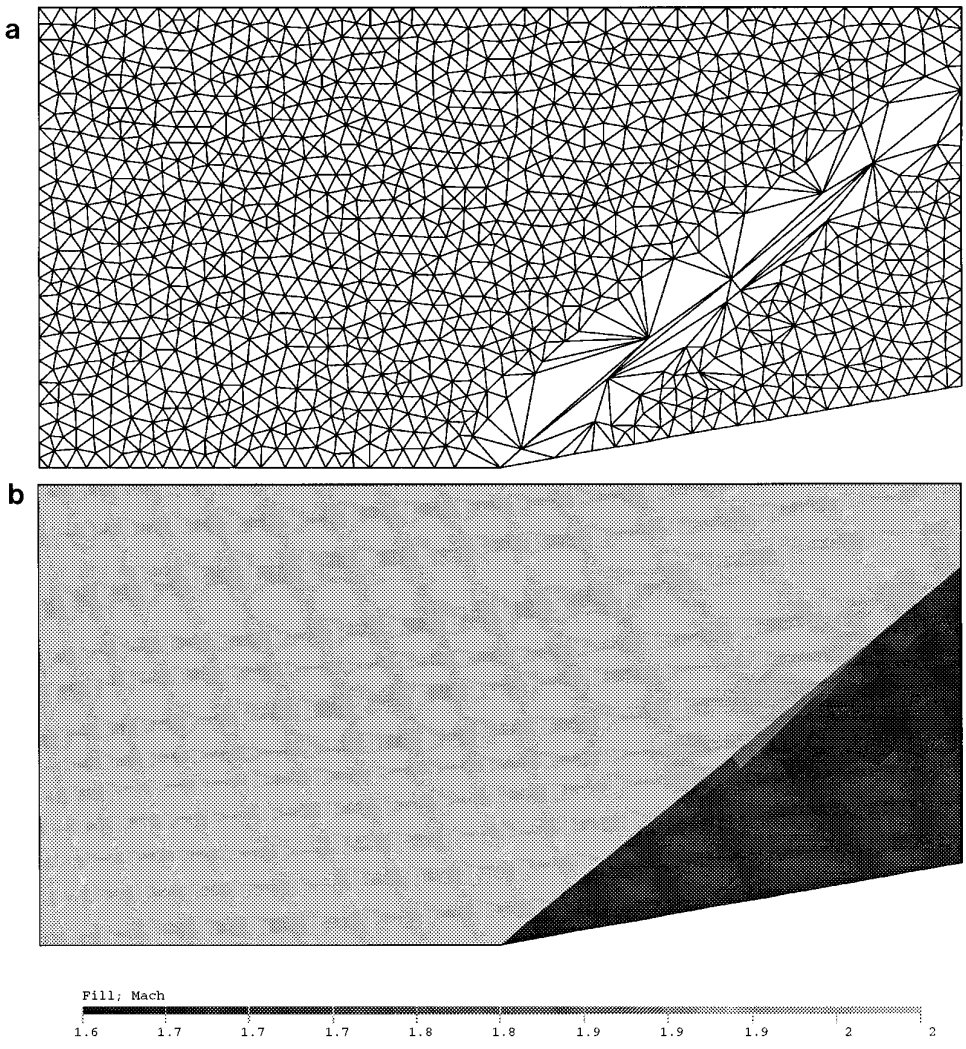

FIG. 6. Converged grid and Mach number distribution using the DDT algorithm and the coarse-cure action.

of the wave model to correctly indicate the wave angle becomes problematic. It is therefore suggested to complement the coarse-cure method by a local refinement procedure.

The third result is used to illustrate the effect of the refinement of the grid. To simplify the analysis, the control of the remeshing is based purely on geometrical data; i.e., the flow has no influence on the refinement. The refinement criteria was the following: a triangle is refined if its area is 1.5 times its reference value, which is the value of the triangle area on the initial grid at the same spatial location. The refinement is performed by bisecting the triangle along its longest side. This ensures that the grid size distribution will remain close to that of the initial grid. The resulting grid and Mach number distribution are presented on Figs. 7a and 7b, respectively. The shock is clearly identified on the grid itself and the Mach number distribution is sharply discontinuous. A more quantitative comparison of the computed pressure distribution is given on Fig. 8. The improvement in the resolution of the discontinuity is noticeable and the figure clearly shows that the analytical solution is well matched for this case.

The convergence of the whole process is an important issue of any adaptation scheme. Figure 9 illustrates the convergence properties of the complete DDT algorithm, including the coarse-cure and refinement actions. The figure presents the number of triangles added (or removed) from the triangulation during each remeshing (the number includes both the cure and refinement actions) versus the iteration number. The cure and refinement actions were carried out every 10 iterations for this problem. Although the plot shows some oscillations in the total number of triangles during the adaptation process, the number of triangles involved is fairly small at each iteration and the process converges after 70 remeshings.

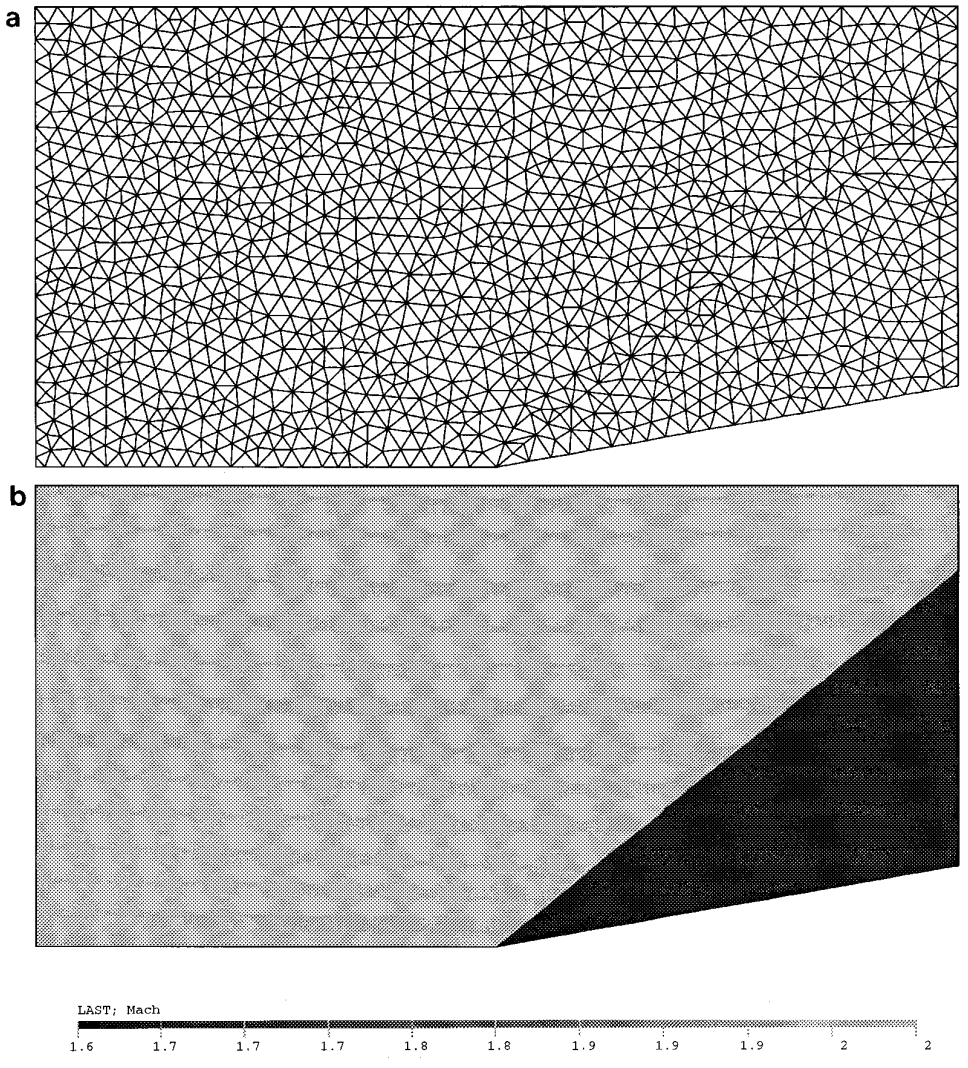

FIG. 7. Converged grid and Mach number distribution using the DDT algorithm with combined coarse-cure and refinement based on area.

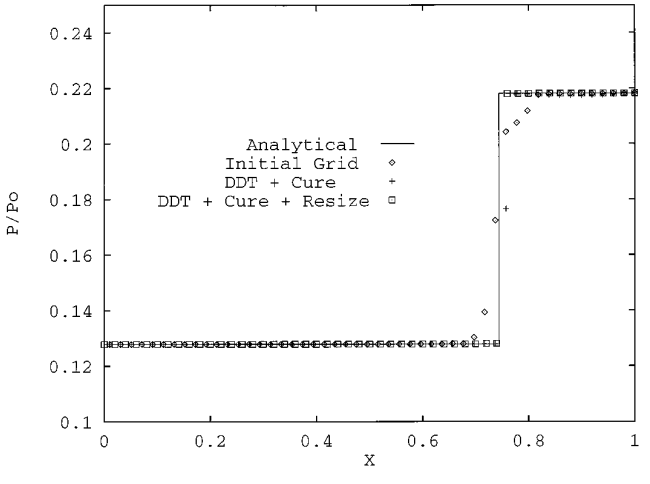

FIG. 8. Comparison of pressure distribution on the line $y = 0.2$ for the various adaptation schemes.

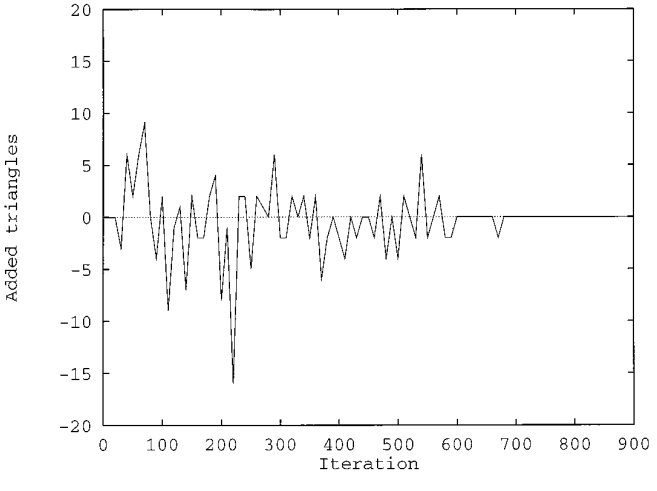

FIG. 9. Convergence of the DDT algorithm.

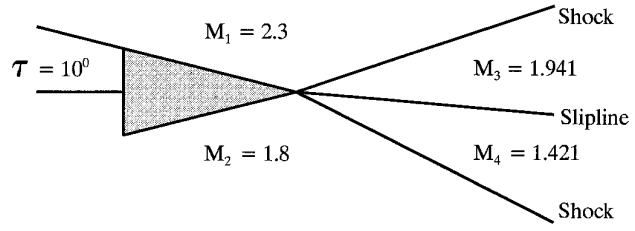

FIG. 10. Schematic description of the confluent supersonic streams problem.

5.2. *Confluent Supersonic Streams*

A second test case was designed to investigate the performance of the DDT method for the detection of slip lines. The problem chosen for this test is the confluence of two supersonic streams of different Mach numbers which generates two shocks and a slip line as illustrated in Fig. 10. The initial grid and the Mach number distribution are shown on Fig. 11. Both shocks and the slip line are visible but are diffused by the scheme. The DDT algorithm was applied to this problem starting from the previous solution. The grid cure and adaptation based on the area were allowed, as described for the first problem. The remeshing was performed every 20 iterations of the flow solution. The results are depicted on Fig. 12.

The difficulty with this case is to identify the origin of the shocks and the slip line at the trailing edge. This can be easily understood since the number of cells surrounding this point is arbitrary and the wave model cannot distinguish all the three distinct waves. However, away from this point, the method is able to detect the waves properly, although the slip line is more difficult to locate accurately. This was also reported in Ref. [3], where the capture of the slip line required 10 times more iterations than the shocks. The results with and without DDT are compared at the exit plane with the analytical solution and are shown in Fig. 13. It can be appreciated that the DDT method is able to reduce by an appreciable amount the diffusion of discontinuities.

5.3. *The One-Dimensional Shock-Tube-Problem*

The third test case chosen is the well-known shock-tube problem, whose solution involves the presence of a moving shock and a contact discontinuity. Although the case is

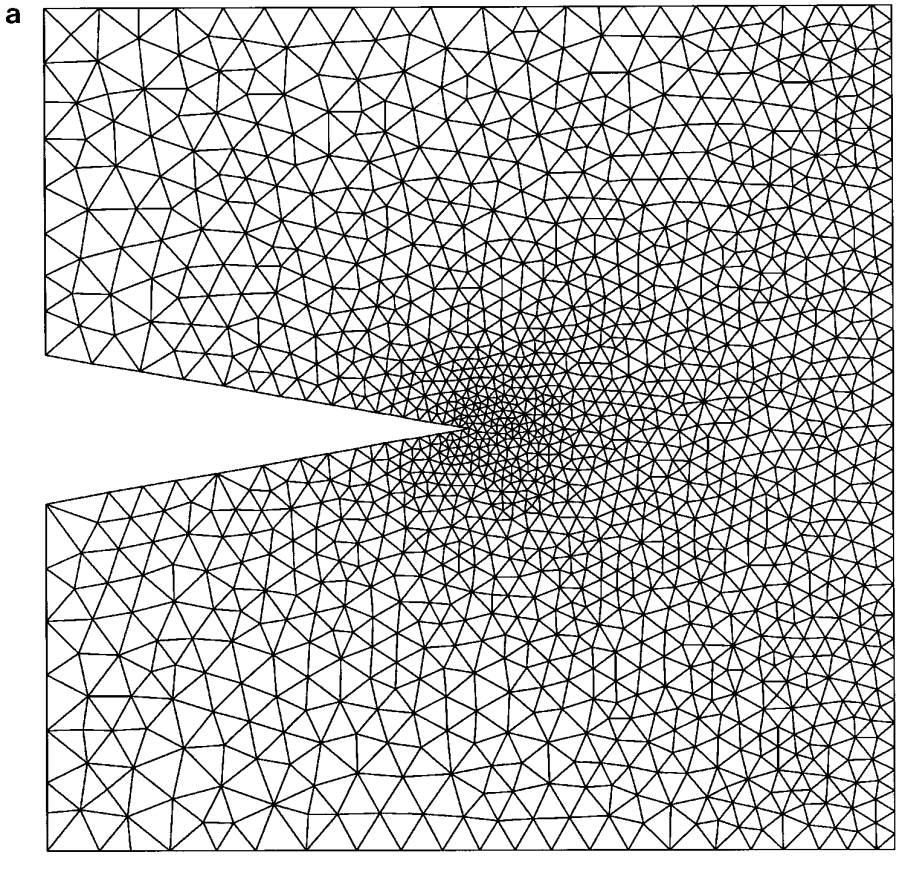

FIG. 11. Initial grid and Mach number distribution for the confluent supersonic streams.

one-dimensional, the problem has been solved using a two-dimensional grid.

The initial condition used is

$$\begin{pmatrix} P \\ T \\ u \end{pmatrix} = \begin{pmatrix} 10 \\ 1 \\ 0 \end{pmatrix} \quad \text{for } x < x_d$$

$$\begin{pmatrix} P \\ T \\ u \end{pmatrix} = \begin{pmatrix} 1 \\ 1 \\ 0 \end{pmatrix} \quad \text{for } x \geq x_d.$$

The performance of the DDT algorithm is first investigated with an initial solution obtained by the standard Roe's scheme on a fixed grid until $T = 10$. Such an initial solution is somewhat diffused, especially at the shock and contact discontinuities which are captured over a few grid points. Using this solution as an initial condition for the DDT method, the computation was carried out until $T = 15$. The results are illustrated in Fig. 14. One can appreciate the ability of the method to recapture the shock wave, which is resolved exactly at the interface between two elements. However, in unsteady situations, the contact discontinuity is not restored by the DDT method, because the characteristics in this region are constants and not converging. Thus, the method is only capable of limiting the diffusion to that already present in the initial solution. If one now repeats the solution procedure using the analytical solution at $T = 10$ as the initial solution and one applies the DDT algorithm until $T = 15$, the results with regards to the contact discontinuity are much better as illustrated on Fig. 14. This again demonstrates that the DDT can detect and maintain a degenerated discontinuity as well as a shock.

6. CONCLUSION

A methodology has been described which allows discontinuities formed during the solution of the Euler equations to be represented exactly at the interfaces of two control

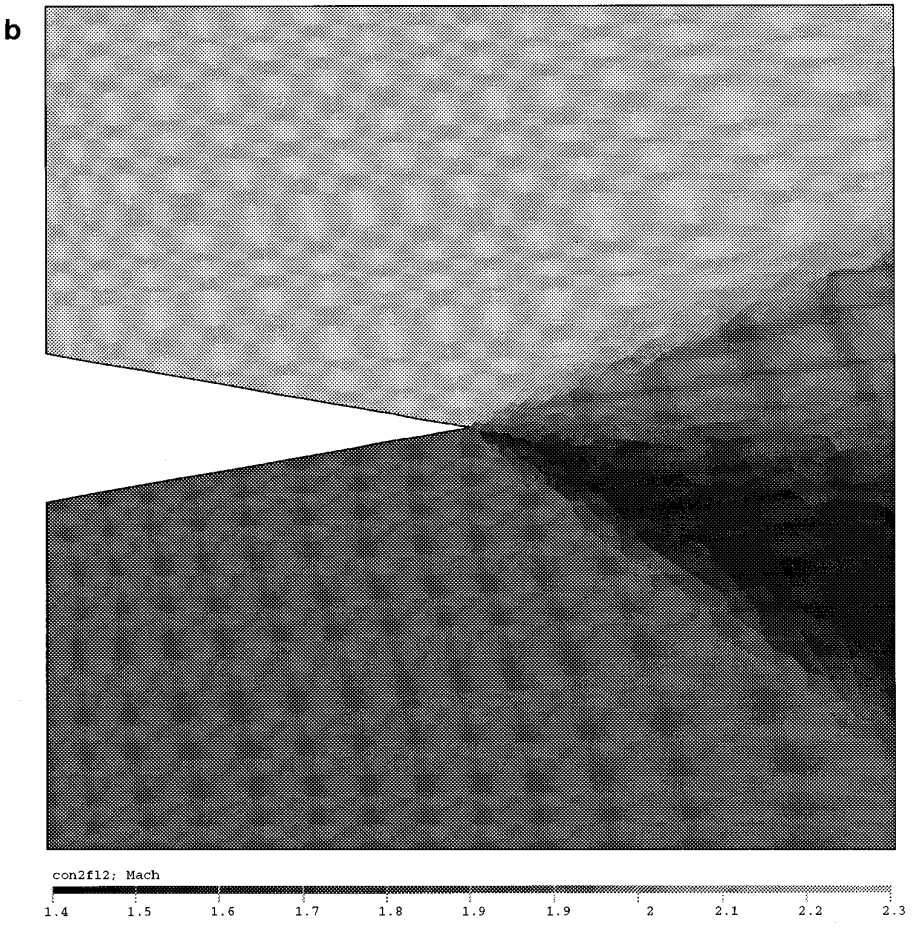

FIG. 11—*Continued*

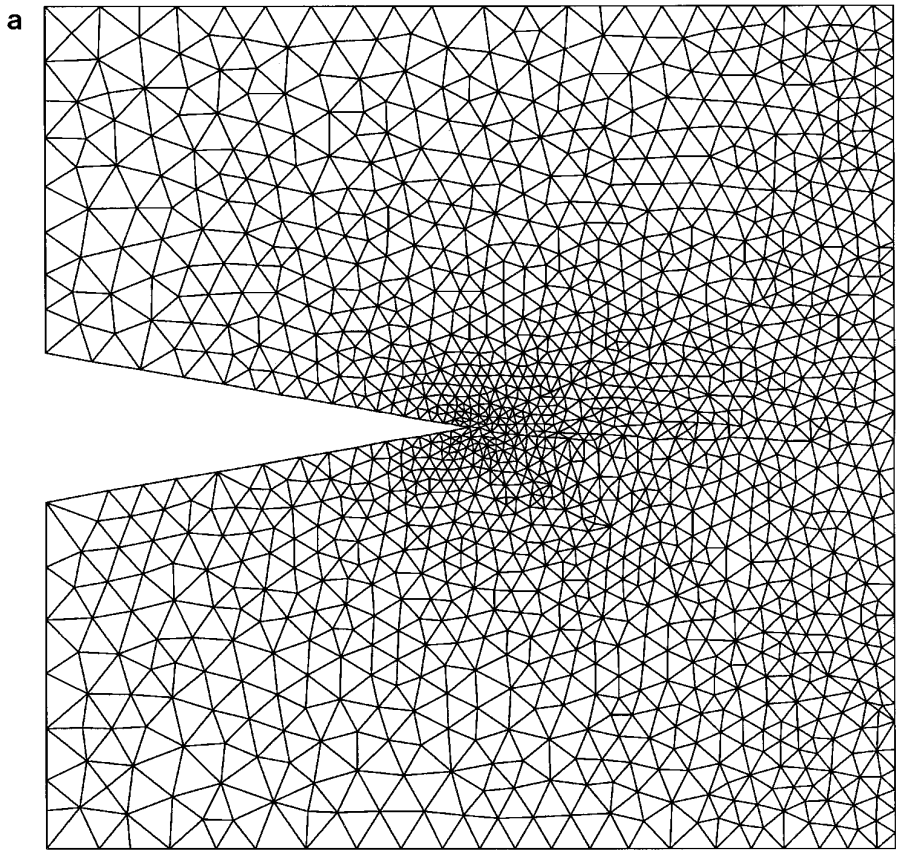

FIG. 12. Converged grid and Mach number distribution for the confluent supersonic streams problem using the DDT algorithm with coarse-cure and refinement based on area.

volumes of a finite-volume method, and this is the result of the application of a standard shock-capturing scheme. It has been shown that the method works very well for capturing stationary or moving shocks and can also represent steady slip lines exactly. The method also minimizes the damping of moving contact discontinuities. The future work includes the extension of the method to three dimensions. In this respect, the main difficulties will lie in the grid cure actions needed to keep a grid of good quality. It is suggested that this method could be used advantageously

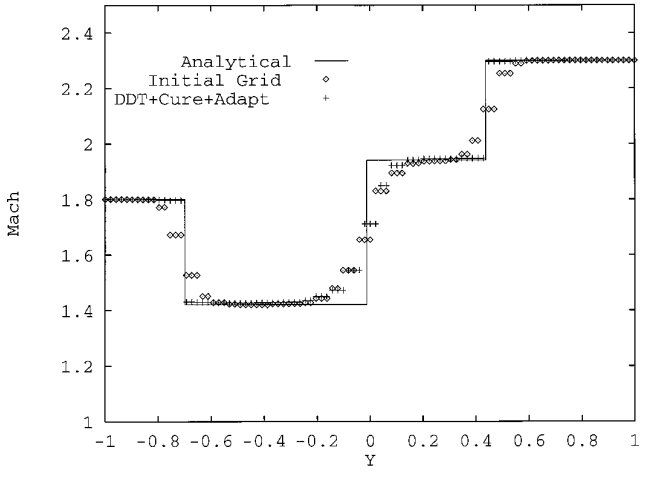

FIG. 13. Comparison of the density profile at the exit plane for the confluent supersonic streams.

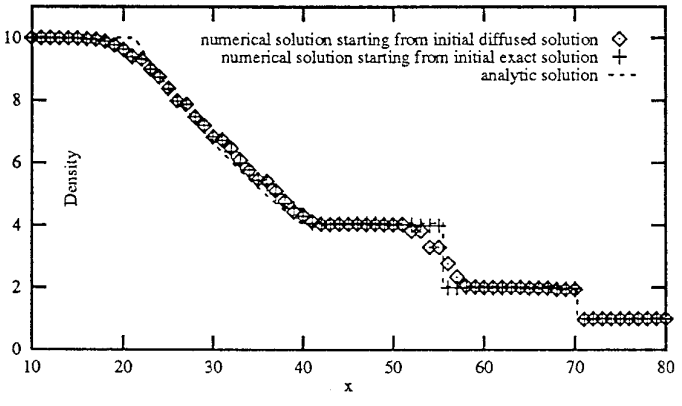

FIG. 14. Results of various methods for the shock tube problem.

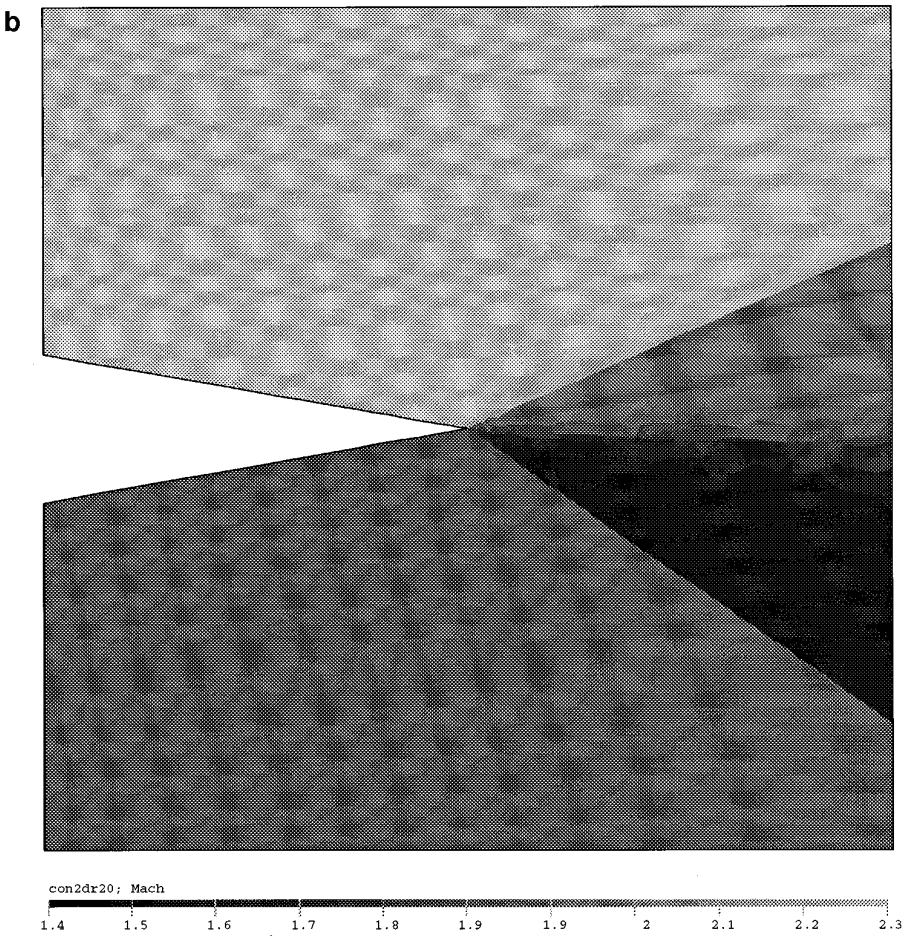

FIG. 12—*Continued*

as an adaptation technique to minimize the number of points required to represent a discontinuity. This could be especially advantageous in three dimensions.

REFERENCES

1. G. Moretti, PIBAL Report No. 73-18, Polytechnique Institute of Brooklyn, Aug. 1973 (unpublished).
2. G. Moretti, *Annu. Rev. Fluid Mech.* 313 (1987).
3. M. Paraschivoiu, J.-Y. Trépanier, M. Reggio, and R. Camarero, AIAA Paper 94-0081, Reno, January 1994 (unpublished).
4. J. Van Rosendale, *ICASE Res. Quart.* **3**(3), 3 (1994).
5. P. L. Roe, *J. Comput. Phys.* **43**(2), 357 (1981).
6. P. L. Roe, *J. Comput. Phys.* **63,** 458 (1986).
7. J.-Y. Trépanier, M. Reggio, H. Zhang, and R. Camarero, *Comput. Fluids* **20**(4), 399 (1981).
8. H. Zhang, M. Reggio, J.-Y. Trépanier, and R. Camarero, *Comput. Fluids* **22**(1), 9 (1993).
9. J.-Y. Trépanier, and H. Yang, École Polytechnique de Montréal, Technical Report. EPM/RT-93/3 (unpublished).
10. H. Zhang and J.-Y. Trépanier, *Int. J. Numer. Methods Eng.* **37,** 1481 (1994).
11. M. Paraschivoiu, M.Sc.A. thesis, Ecole Polytechnique de Montréal, 1993 (unpublished).